Acta Cryst. (1997). B53, 822–830

Definitive Structural Characterization of the Conventional Low-Temperature Host Structure in Urea Inclusion Compounds

LILY YEO AND KENNETH D. M. HARRIS*

School of Chemistry, University of Birmingham, Edgbaston, Birmingham B15 2TT, England. E-mail: k.d.m.harris@bham.ac.uk

(Received 11 December 1996; accepted 8 April 1997)

Abstract

Structural properties of the 1,10-dibromodecane/urea and 1,12-dibromododecane/urea inclusion compounds have been determined by single crystal X-ray diffraction for both the high- and low-temperature phases. In the high-temperature phase both inclusion compounds have the conventional hexagonal urea tunnel structure, with substantial orientational disorder of the guest molecules. In the low-temperature phase the urea tunnel structure distorts to an orthorhombic structure, based on a distorted form of the orthohexaganol cell of the high-temperature structure and with the loss of the *C* centre. Within this tunnel structure there is evidence that the guest molecules have a narrow distribution of orientations (with respect to rotation about the tunnel axis) and the preferred orientation of the guest molecules correlates well with the observed distortion of the host tunnel. This represents the first accurate and reliable report of the conventional low-temperature structure of urea inclusion compounds. Previous powder X-ray diffraction studies have confirmed that the host structure in the low-temperature phase of 1,10-dibromodecane/urea is the same as that in the low-temperature phase of the alkane/urea inclusion compounds.

1. Introduction

In recent years there has been considerable interest in urea inclusion compounds (Hollingsworth & Harris, 1996; Harris, 1993), in recognition of the fact that these solids exhibit a diverse range of interesting and important physico-chemical properties. In these solids the urea molecules form an extensively hydrogen-bonded host structure (Smith, 1952; Harris & Thomas, 1990), containing linear parallel tunnels, with guest molecules packed densely along these tunnels. One of the most widely studied, although at the same time one of the least well understood, aspects of urea inclusion compounds concerns the phase transition that occurs in these solids at sufficiently low temperature [for example, at ~ 150 K for hexadecane/urea (Harris, Gameson & Thomas, 1990) and at ~ 143 K for 1,10-dibromodecane/urea (Aliev, Smart, Shannon & Harris, 1996)]. This transition was first observed from heat capacity data for urea inclusion compounds containing alkane guest molecules (Pemberton & Parsonage, 1965, 1966) and was subsequently shown to involve both a distortion of the urea tunnel structure to lower symmetry (Chatani, Taki & Tadokoro, 1977; Chatani, Anraku & Taki, 1978; Harris, Gameson & Thomas, 1990; Aliev, Smart, Shannon & Harris, 1996), hexagonal above and orthorhombic below the phase transition temperature, and a change in the dynamics of the guest molecules (Casal, Cameron & Kelusky, 1984; Harris & Jonsen, 1989; Guillaume, Sourisseau & Dianoux, 1991; Smart, Guillaume, Harris & Dianoux, 1994; Aliev, Smart, Shannon & Harris, 1996; El Baghdadi, Dufourc & Guillaume, 1996) with the motional freedom generally becoming reduced substantially below the phase transition temperature.

To understand the fundamental nature of urea inclusion compounds it is clearly essential to understand the low-temperature phase transition and so accurate knowledge of the structural properties in both the low- and high-temperature phases is crucial. So far, three models (Parsonage & Pemberton, 1967; Fukao, 1990; Lynden-Bell, 1993) have been proposed to account for the phase transition. Of these models only the translation–rotation coupling model of Lynden-Bell (Lynden-Bell, 1993) takes due cognisance of the fact that the host structure is different in the low- and high-temperature phases, and for this reason, among others, this model is the most consistent with current experimental evidence. In spite of this recent progress, however, several aspects of the phase transition in urea inclusion compounds remain to be comprehensively understood and the development of a fundamental understanding of the mechanism for the phase transition is still one of the major challenges in this field.

Clearly a detailed rationalization of the phase transition requires, *inter alia*, that the structural properties of both the high- and low-temperature phases are well understood. For the high-temperature phase, single crystal X-ray diffraction studies have led to accurate

information on the (average) host structures of urea inclusion compounds containing a wide range of guest molecules. With the exception of a few special cases (Hollingsworth, Santarsiero & Harris, 1994; Brown & Hollingsworth, 1995; Brown, Chaney, Santarsiero & Hollingsworth, 1996; Hollingsworth, Brown, Hillier, Santarsiero & Chaney, 1996; Hollingsworth *et al.*, 1997), in which the relationship between the host and guest structures is commensurate, all urea inclusion compounds have the 'conventional' urea tunnel structure (space group $P6_122$; $a \simeq 8.2$, $c \simeq 11.0$ Å) shown in Fig. 1 in the high-temperature phase (which generally includes ambient temperature). For the low-temperature phase, on the other hand, definitive structural characterization of the host structure has encountered major difficulties, because a single crystal of the urea inclusion compound in the high-temperature phase (for example, produced directly by crystal growth around ambient temperature) generally becomes multiply twinned on passing below the phase transition temperature. Thus, the distortion that lowers the symmetry from hexagonal to orthorhombic on passing below the phase transition temperature can occur in three ways that are orientationally distinct, but equivalent with respect to the parent hexagonal structure. Clearly if the transition is initiated independently in different regions of the parent hexagonal crystal, a multiply twinned crystal will be produced on entering the low-temperature phase, whereas if the distortion of the host structure is initiated at one point in the parent hexagonal crystal and propagates cooperatively throughout this crystal, then the single crystal character may be maintained on entering the low-temperature phase. Unfortunately, the former situation has pertained in previous attempts to determine the conventional low-temperature structure of urea inclusion compounds by single crystal X-ray diffraction. There has been only one reported structure determination of the low-temperature phase (Chatani, Taki & Tadokoro, 1977), from poor-quality single crystal diffraction data (affected significantly by the problem of crystal twinning) for the hexadecane/urea inclusion compound. Although this work led to a qualitative understanding of the host structure in the low-temperature phase [see also Chatani, Anraku & Taki (1978)], including the fact that it is orthorhombic with space group $P2_12_12_1$, no atomic coordinates were actually reported or deposited. Due to the inherent uncertainties and inaccuracies associated with the determination of this structure, a more definitive determination of the low-temperature host structure has long been sought. Powder diffraction has been recognized (Harris, Gameson & Thomas, 1990) as a viable approach, in view of the fact that the powder diffractogram of the low-temperature phase should be unaffected (at least to a first approximation) by the occurrence of crystal twinning. However, attempts to refine the low-temperature host structure by Rietveld refinement, using the structure of the high-temperature phase as the starting point, were not successful.

As alkane/urea inclusion compounds are the prototypical urea inclusion compounds, the low-temperature structure of these inclusion compounds can be considered to represent the 'conventional' low-temperature structure. Powder X-ray diffraction has shown (Aliev, Smart, Shannon & Harris, 1996) that the 1,10-dibromodecane/urea inclusion compound has the same host structure as the alkane/urea inclusion compounds in the low-temperature phase.

As reported below, we have discovered that the 1,10-dibromodecane/urea and 1,12-dibromododecane/urea inclusion compounds (DB10 and DB12 hereafter) remain as single crystals on passing into the low-temperature phase, allowing structural characterization of the low-temperature phase by single crystal X-ray diffraction. As it has been demonstrated previously by powder X-ray diffraction (Aliev, Smart, Shannon & Harris, 1996) that DB10 has the conventional low-temperature host structure exhibited by the alkane/urea inclusion compounds, the results reported here represent the first definitive structural characterization of the conventional low-temperature structure of urea inclusion compounds.

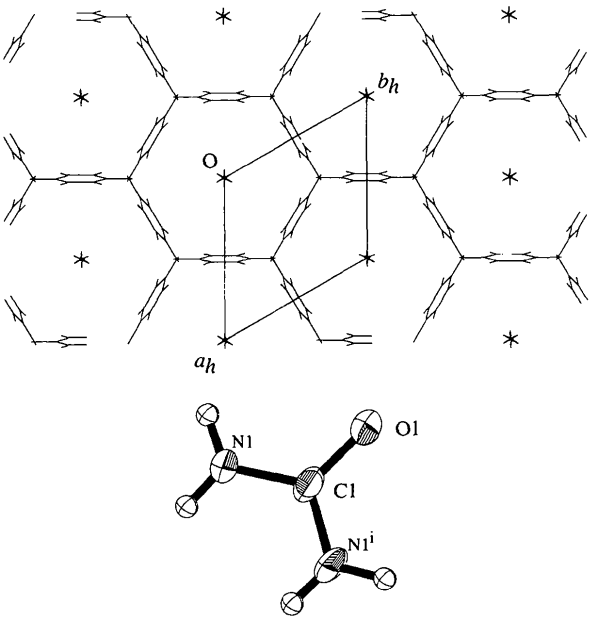

Fig. 1. Structure of the high-temperature phase of DB10 (ambient temperature), viewed along the host tunnel axis (crystallographic c axis). Inset: *ORTEP*II (Johnson, 1976) representation of one urea molecule in the structure, indicating atom labelling. The urea molecule lies on a crystallographic twofold axis. The atoms within the tunnel (C2 and C3) represent the contribution to the 'h' diffraction pattern from scattering by the guest molecules (the physical significance of these atom positions is discussed in the text).

2. Experimental

DB10 and DB12 were prepared from commercially available reagents using the following method. Separate saturated solutions of the α,ω-dibromoalkane in 2-methylbutan-2-ol and urea in methanol were prepared under ultrasonic agitation at ~ 328 K. These solutions were then mixed in a conical flask, in amounts corresponding to an excess of the α,ω-dibromoalkane (excess with respect to the expected guest/host molar ratio in the inclusion compound). Crystals of the inclusion compound that precipitated immediately were dissolved by adding more methanol. The flask was then transferred to an incubator and cooled systematically from 328 to 288 K over a period of 24 h. When sufficiently large crystals had grown (generally after a few days), they were collected and washed with 2,2,4-trimethylpentane. The crystals were long hexagonal needles and their behaviour in the polarizing microscope was consistent with their assignment to the hexagonal crystal system. Powder X-ray diffractograms recorded at ambient temperature confirmed that these crystals had the conventional hexagonal host structure of urea inclusion compounds in the high-temperature phase and indicated that the samples did not contain any significant amount of the crystalline phase of 'pure' urea (the crystal structure of which differs substantially from the urea substructure in urea inclusion compounds).

Single crystal X-ray diffraction experiments used a Rigaku R-Axis II diffractometer with area detector and a standard MSC low-temperature device. (The stability and accuracy of the low-temperature device have been determined to be $\sim \pm 2$ K.) For all experiments at low temperature, the crystals were allowed ~ 2 h to reach thermal equilibrium before starting the X-ray diffraction measurements.

To provide an initial qualitative understanding of the diffraction patterns, single crystal X-ray diffraction oscillation photographs were recorded at ambient temperature and 108 K, with the oscillation axis parallel to the needle axis of the crystal (tunnel axis of the urea host structure). Different crystals were used for the experiments at ambient temperature and low temperature.

For both DB10 and DB12 the data collections at ambient temperature comprised 18 frames, each recorded over an oscillation range of 10° with an exposure time of 10 min per frame, whereas the data collections at low temperature comprised 23 frames, each recorded over an oscillation range of 8° with an exposure time of 10 min per frame. The crystal-to-detector distance was 80 mm in all cases.

3. Resumé of structural properties of conventional urea inclusion compounds

In conventional urea inclusion compounds there is an incommensurate relationship between the periodic repeat distances (denoted c_h and c_g, respectively) of the host and guest substructures along the tunnel axis (classically, for an incommensurate system, sufficiently small integers p and q cannot be found for which $pc_h \simeq qc_g$). Although the host and guest substructures have different structural periodicities, these two substructures are not independent, as each substructure exerts an incommensurate modulation upon the other. Thus, the host substructure is best considered in terms of a 'basic structure' which is subjected to an incommensurate modulation mediated by the guest substructure; the basic structure can be described using conventional crystallographic principles (*e.g.* three-dimensional space group symmetry). Similarly, the guest substructure can be considered in terms of an incommensurately modulated basic structure. The incommensurate modulations describe perturbations to the basic structures that arise as a consequence of the host–guest interaction. A full discussion of these structural issues for urea inclusion compounds is given in Harris & Thomas (1990).

Transforming this structural description into reciprocal space, an incommensurate urea inclusion compound gives two distinguishable diffraction patterns: the 'h' diffraction pattern, which arises from diffraction by the basic host structure (and by the incommensurate modulation within the guest substructure), and the 'g' diffraction pattern, which arises from diffraction by the basic guest structure (and by the incommensurate modulation within the host substructure). The reciprocal lattice defining the positions of maxima in the 'h' diffraction pattern is reciprocal to the direct space lattice that defines the periodicity of the basic host structure and the reciprocal lattice defining the positions of maxima in the 'g' diffraction pattern is reciprocal to the direct space lattice that defines the periodicity of the basic guest structure.

4. Data analysis

The reported data collections at ambient temperature and 108 K constitute measurements of the 'h' diffraction data. As discussed in Harris & Thomas (1990), structure determination calculations using the 'h' diffraction data allow the basic host structure to be determined, as well as providing restricted information on the guest substructure, as now described for the case in which the c axis is parallel to the tunnel axis. First, the $hk0$ reflections (which are common to both the 'h' and 'g' diffraction patterns) provide two-dimensional information on the basic guest structure projected onto the plane perpendicular to the tunnel axis. Second, the 'h' reflections $(hkl)_h$ with $l \neq 0$ convey information on the incommensurate perturbations to the basic guest structure (these perturbations, which arise from the host–guest interaction, have the same periodicity as the basic host structure). This 'perturbation electron density' represents the difference in electron density

between the true guest substructure averaged over the periodicity of the basic host structure and the basic guest structure averaged over the periodicity of the basic host structure. Although this 'perturbation electron density' conveys important structural information, it is more satisfactory to seek a comprehensive understanding of the incommensurate modulations in incommensurate inclusion compounds by structure determination of the composite inclusion compound in a four-dimensional superspace group (van Smaalen, 1995; van Smaalen & Harris, 1996; Lefort, Etrillard, Toudic, Guillaume, Breczewski & Bourges, 1996), considering together the '*h*' diffraction data, the '*g*' diffraction data and any additional satellite reflections. Unfortunately, the opportunities for such analysis in the present case are limited, *inter alia*, by the fact that there are only very few Bragg diffraction maxima of significant intensity in the '*g*' diffraction pattern.

In this paper we focus on the analysis of the '*h*' diffraction pattern. In summary, structure determination calculations using the '*h*' diffraction data yield the following information: (*a*) the average basic host structure and (*b*) an average guest electron distribution, which has a straightforward physical interpretation when projected onto the plane perpendicular to the tunnel axis.

In structure refinement the method of introducing the contributions from the guest electron density requires special attention and the following strategy was followed in the present work. For the non-H atoms of urea, positional parameters (taken initially from the results of the structure solution calculation) and anisotropic atomic displacement parameters were refined in the conventional manner. The difference-Fourier map for this 'host-only' structural model contained significant maxima located within the tunnel, clearly representing guest electron density. A C atom was added in the position of the highest maximum in the difference-Fourier map and its positional parameters and isotropic atomic displacement parameter were refined together with the parameters for the non-H atoms of the host structure (as expected, the refined values of the isotropic atomic displacement parameters for the C atoms in the tunnel are significantly higher than the equivalent isotropic atomic displacement parameters for the atoms of the urea molecules). This procedure was repeated, adding one C atom at a time, until the highest peak in the difference-Fourier map represented the position of a urea H atom. Finally, H atoms were added to the urea molecules according to standard geometric features and refined using a 'riding' model (*i.e.* the coordinate shifts for the H atom and the N atom to which it is attached are the same). The isotropic atomic displacement parameter of each H atom was refined as 1.2 times the equivalent isotropic atomic displacement parameter of the nitrogen atom to which it is attached.

Structure solution calculations were carried out using the direct methods program *SIR*92 (Burla *et al.*, 1989) and structure refinement calculations were carried out using the *SHELX*93 (Sheldrick, 1993) program. Standard agreement factors R and wR were considered.

5. Results and discussion

Single crystal X-ray diffraction oscillation photographs recorded at ambient temperature for DB10 and DB12 are shown in Figs. 2(*a*) and 2(*b*), and can be interpreted on the basis of the '*h*' and '*g*' diffraction patterns discussed previously (Harris & Thomas, 1990) for urea inclusion compounds. Structural parameters determined from the measured '*h*' diffraction data (see §4) are given in Table 2 (where RT = room temperature and LT = low temperature), and bond lengths and angles are summarized in Table 3. The structure determined for DB10 is shown in Fig. 1.† Clearly these urea inclusion compounds have the conventional urea tunnel structure in the high-temperature phase.

From the oscillation photographs shown in Figs. 2(*a*) and 2(*b*), it can be inferred that the basic guest structures in DB10 and DB12 are characterized by the relationship $\Delta_g = c_g/3$ (Δ_g is the offset along the tunnel axis between the centres of mass of guest molecules in adjacent tunnels) established previously (Harris, Smart & Hollingsworth, 1991) for α,ω-dibromoalkane/urea inclusion compounds. The diffuse scattering (in high index layers) in the '*g*' diffraction pattern suggests that there is some loss of three-dimensional ordering of the guest molecules in directions perpendicular to the tunnel axis.

We now consider the structural properties of the low-temperature phase. Single crystal oscillation photographs recorded at 108 K for DB10 and DB12 are shown in Figs. 2(*c*) and 2(*d*), respectively. There is no evidence for the generation of any superstructures along the tunnel direction (*i.e.* no new layer lines appear in the oscillation photograph). However, for both inclusion compounds, the '*h*' diffraction pattern at 108 K is different from that at ambient temperature, particularly in terms of the number and arrangement of discrete diffraction maxima within the layer lines. These facts are accounted for completely by the structural properties discussed below. The structures determined from the '*h*' diffraction data recorded at 108 K for DB10 and DB12 are viewed along the tunnel axis in Figs. 3(*a*) and 3(*b*), and the structural parameters are given in Table 2.

The average basic host structures for the DB10 and DB12 inclusion compounds at 108 K are the same within estimated experimental errors in the determination of the structural parameters. As verified previously by powder X-ray diffraction (see §1), these structures are also the

† Lists of atomic coordinates, anisotropic displacement parameters and structure factors have been deposited with the IUCr (Reference: HA0155). Copies may be obtained through The Managing Editor, International Union of Crystallography, 5 Abbey Square, Chester CH1 2HU, England.

same as the average basic host structure in the low-temperature phase of alkane/urea inclusion compounds. The orthorhombic low-temperature structure is based on a distortion of the hexagonal high-temperature structure and is based approximately on the orthohexagonal lattice of the high-temperature phase, but with the loss of the *C* centre. The extent of distortion is relatively small, as evident by comparison of Tables 2 and 4. The two tunnels running through the unit cell in the low-temperature phase (see Fig. 3) are structurally identical (related by twofold screw axes). As shown in Fig. 3, the projection of these tunnels onto the plane perpendicular to the tunnel axis is a distorted hexagon with one 'diameter' between opposite corners of the hexagon longer than the other two diameters. The guest molecules exhibit a well-defined orientational preference which correlates well with the distortion of the host tunnel; thus, the plane of the guest molecule (projected onto the plane perpendicular to the tunnel axis) lies along the long diameter of the distorted host tunnel. Clearly the orientation of the guest molecule with respect to rotation about the tunnel axis is confined to a narrow distribution in the low-temperature phase, consistent with conclusions that may be drawn from the known

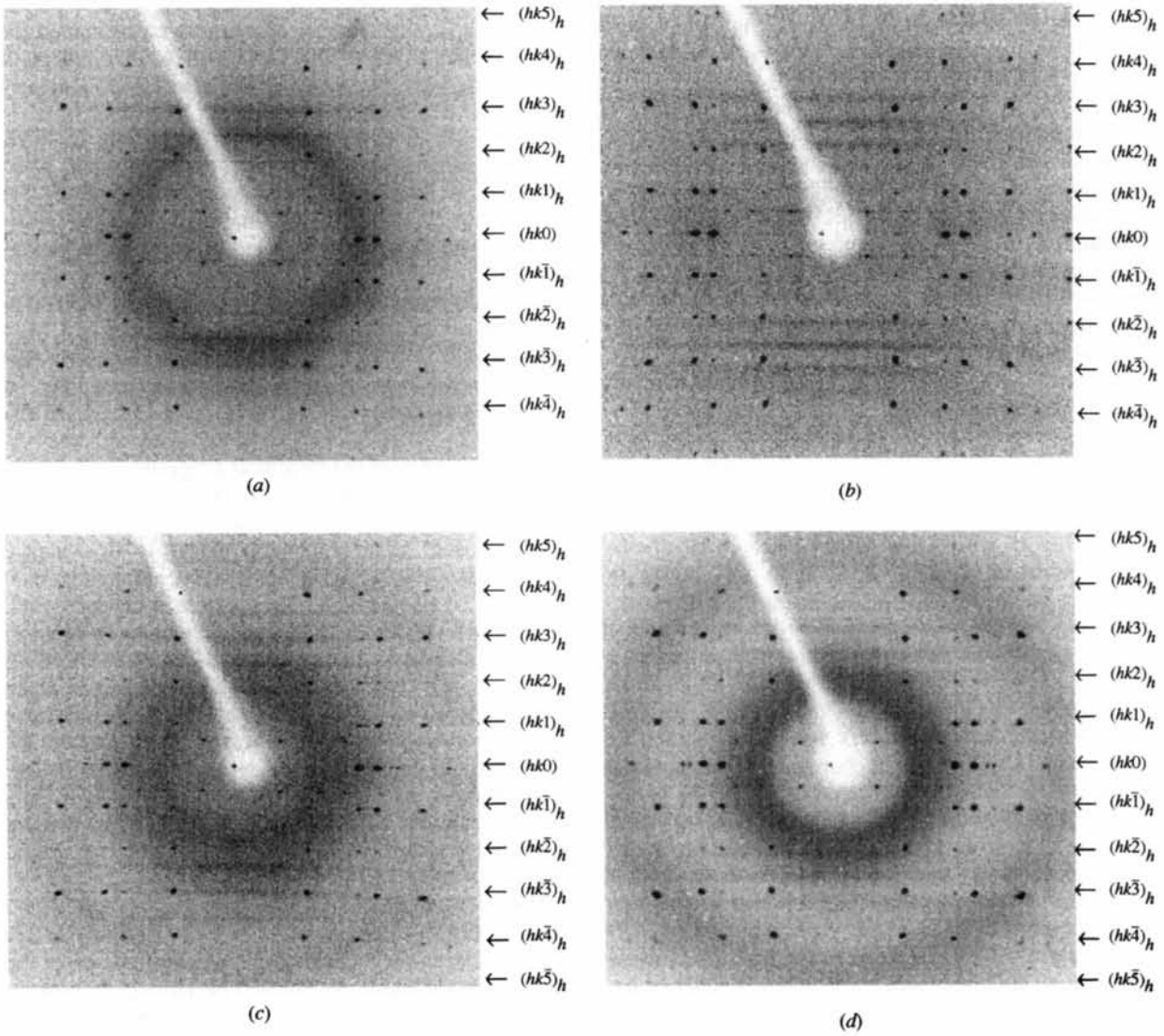

Fig. 2. Single crystal oscillation photographs for urea inclusion compounds oscillating about the tunnel axis (oscillation range 120°). Layer lines of the '*h*' diffraction pattern are indexed (the X-ray scattering between these layers represents the '*g*' diffraction pattern and comprises both discrete and diffuse scattering). (*a*) DB10 at ambient temperature, (*b*) DB12 at ambient temperature, (*c*) DB10 at 108 K and (*d*) DB12 at 108 K. [The indices shown in (*c*) and (*d*) correspond to a cell for the low-temperature phase with the c_h axis as the tunnel axis (note that in the discussion of this structure later in the text, the a_h axis is the tunnel axis).]

Table 1. *Experimental details*

	DB10 RT	DB12 RT	DB10 LT	DB12 LT
Crystal data				
Cell setting	Hexagonal	Hexagonal	Orthorhombic	Orthorhombic
Space group	$P6_122$	$P6_122$	$P2_12_12_1$	$P2_12_12_1$
a (Å)	8.271 (3)	8.2201 (13)	11.007 (2)	10.930 (2)
b (Å)			13.945 (4)	14.133 (3)
c (Å)	11.083 (3)	11.0342 (12)	8.080 (2)	8.186 (2)
V (Å^3)	656.7 (4)	645.7 (2)	1240.2 (5)	1264.5 (4)
Z	6	6	12	12
D_x (Mg m^{-3})	1.276	1.297	1.415	1.388
Radiation type	Mo $K\alpha$	Mo $K\alpha$	Mo $K\alpha$	Mo $K\alpha$
Wavelength (Å)	0.71069	0.71069	0.71069	0.71069
No. of reflections for cell parameters	3351 (post-refined using complete data set)	3714 (post-refined using complete data set)	6613 (post-refined using complete data set)	6710 (post-refined using complete data set)
θ range (°)	2.5–50.21	2.5–50.64	2.5–50.90	2.5–50.58
μ (mm^{-1})	0.90	1.09	0.96	1.217
Temperature (K)	293 (2)	293 (2)	108 (2)	108 (2)
Crystal form	Hexagonal needle	Hexagonal needle	Hexagonal needle	Hexagonal needle
Crystal size (mm)	0.4 × 0.3 × 0.3	0.4 × 0.3 × 0.3	0.4 × 0.3 × 0.3	0.4 × 0.3 × 0.3
Crystal colour	Colourless	Colourless	Colourless	Colourless
Data collection				
Diffractometer	Rigaku R-AxisII area detector	Rigaku R-AxisII area detector	Rigaku R-AxisII area detector	Rigaku R-AxisII area detector
Data collection method	Image plate scans	Image plate scans	Image plate scans	Image plate scans
Absorption correction	None	None	None	None
No. of measured reflections	3351	3714	6613	6610
No. of independent reflections	393	395	2181	2195
No. of observed reflections	384	387	1860	1940
Criterion for observed reflections	$I > 2\sigma(I)$	$I > 2\sigma(I)$	$I > 2\sigma(I)$	$I > 2\sigma(I)$
R_{int}	0.1054	0.0840	0.0844	0.0731
θ_{max} (°)	25.10	25.32	25.45	25.29
Range of h, k, l	$-9 \rightarrow h \rightarrow 9$ $-9 \rightarrow k \rightarrow 9$ $-12 \rightarrow l \rightarrow 13$	$-9 \rightarrow h \rightarrow 9$ $-9 \rightarrow k \rightarrow 9$ $-12 \rightarrow l \rightarrow 12$	$-13 \rightarrow h \rightarrow 13$ $-16 \rightarrow k \rightarrow 16$ $-9 \rightarrow l \rightarrow 9$	$-12 \rightarrow h \rightarrow 12$ $-16 \rightarrow k \rightarrow 16$ $-9 \rightarrow l \rightarrow 9$
Refinement				
Refinement on	F^2	F^2	F^2	F^2
$R[F^2 > 2\sigma(F^2)]$	0.1133	0.1099	0.1354	0.1234
$wR(F^2)$	0.2915	0.3018	0.3313	0.3448
S	1.230	1.220	1.111	1.036
No. of reflections used in refinement	393	395	2181	2195
No. of parameters used	24	24	137	137
H-atom treatment	H atoms were added to the urea molecules according to standard geometry and refined using a 'riding' model. The U_{iso} of each H atom was refined as 1.2 times the equivalent isotropic atomic displacement of the N atom to which it is attached.	H atoms were added to the urea molecules according to standard geometry and refined using a 'riding' model. The U_{iso} of each H atom was refined as 1.2 times the equivalent isotropic atomic displacement of the N atom to which it is attached.	H atoms were added to the urea molecules according to standard geometry and refined using a 'riding' model. The U_{iso} of each H atom was refined as 1.2 times the equivalent isotropic atomic displacement of the N atom to which it is attached.	H atoms were added to the urea molecules according to standard geometry and refined using a 'riding' model. The U_{iso} of each H atom was refined as 1.2 times the equivalent isotropic atomic displacement of the N atom to which it is attached.
Weighting scheme	$w = 1/[\sigma^2(F_o^2) + (0.1184P)^2 + 1.4180P]$, where $P = (F_o^2 + 2F_c^2)/3$	$w = 1/[\sigma^2(F_o^2) + (0.1447P)^2 + 1.0780P]$, where $P = (F_o^2 + 2F_c^2)/3$	$w = 1/[\sigma^2(F_o^2) + (0.1141P)^2 + 6.3476P]$, where $P = (F_o^2 + 2F_c^2)/3$	$w = 1/[\sigma^2(F_o^2) + (0.1876P)^2 + 3.5933P]$, where $P = (F_o^2 + 2F_c^2)/3$
$(\Delta/\sigma)_{max}$	0.001	0.000	0.075	0.282
$\Delta\rho_{max}$ (e Å^{-3})	0.327	0.327	0.494	0.501
$\Delta\rho_{min}$ (e Å^{-3})	−0.159	−0.200	−0.512	−0.381
Extinction method	None	None	None	None
Source of atomic scattering factors	*International Tables for Crystallography* (1992, Vol. C)	*International Tables for Crystallography* (1992, Vol. C)	*International Tables for Crystallography* (1992, Vol. C)	*International Tables for Crystallography* (1992, Vol. C)
Absolute configuration	Flack (1983)	Flack (1983)	Flack (1983)	Flack (1983)
Computer programs				
Data collection	*R-Axis*II software (Rigaku, 1994)	*R-Axis*II software (Rigaku, 1994)	*R-Axis*II software (Rigaku, 1994)	*R-Axis*II software (Rigaku, 1994)
Cell refinement	*R-Axis*II software (Rigaku, 1994)	*R-Axis*II software (Rigaku, 1994)	*R-Axis*II software (Rigaku, 1994)	*R-Axis*II software (Rigaku, 1994)
Data reduction	*TEXSAN* (Molecular Structure Corporation, 1993)	*TEXSAN* (Molecular Structure Corporation, 1993)	*TEXSAN* (Molecular Structure Corporation, 1993)	*TEXSAN* (Molecular Structure Corporation, 1993)
Structure solution	*TEXSAN* (Molecular Structure Corporation, 1993)	*TEXSAN* (Molecular Structure Corporation, 1993)	*TEXSAN* (Molecular Structure Corporation, 1993)	*TEXSAN* (Molecular Structure Corporation, 1993)
Structure refinement	*SHELXL93* (Sheldrick, 1993)	*SHELXL93* (Sheldrick, 1993)	*SHELXL93* (Sheldrick, 1993)	*SHELXL93* (Sheldrick, 1993)
Preparation of material for publication	*SHELXL93* (Sheldrick, 1993)	*SHELXL93* (Sheldrick, 1993)	*SHELXL93* (Sheldrick, 1993)	*SHELXL93* (Sheldrick, 1993)

differences between the dynamic properties of the guest molecules in the high- and low-temperature phases.

It is interesting to note that in the '*h*' diffraction data recorded for both DB10 and BD12 at 108 K, all reflections of the type *hk*0 with *k* odd are absent, implying the following (approximate) condition for the presence of reflections: *hk*0, $k = 2n$. This condition suggests that the structure should have a *b* glide plane perpendicular to the *c* axis and is in addition to the three conditions characteristic of space group $P2_12_12_1$, *i.e.* *h*00, $h = 2n$; 0*k*0, $k = 2n$; 00*l*, $l = 2n$. However, none of the orthorhombic space groups has only these four conditions for the presence of reflections and the structure clearly does not possess a *b* glide plane perpendicular to the *c* axis. The observed condition for the *hk*0 reflections is related to the fact that the low-temperature host structure is only slightly distorted from *A*-centred orthorhombic (the orthohexagonal description of the host structure in the high-temperature phase is a centred orthorhombic cell and the setting used here for the low-temperature phase would correspond to an *A* centre). However, the presence of an *A* centre dictates that *hkl* reflections should be observed only for $k + l$ even, with this condition holding for all values of *l*, whereas in the present case this condition apparently holds strictly only when $l = 0$. Thus, for $l \neq 0$ several reflections with $k + l$ odd have significant intensity, although it is true that those with $k + l$ odd are generally less intense than those with $k + l$ even, consistent with the fact that the structure is distorted only slightly from *A*-centred. Clearly, the observed condition that *hk*0 reflections are absent for *k* odd is derived from the fact that the structure is only slightly distorted from *A*-centred, although the differences in behaviour for reflections with $l = 0$ and $l \neq 0$ suggests a more subtle dependence on the exact way in which the low-temperature structure is distorted from *A*-centred orthorhombic. This discussion highlights an interesting example in which inspection of the diffraction data reveals systematic absences that are characteristic of a particular symmetry element (*b*-glide plane), even though that symmetry element is not actually present (not even approximately) in the structure.

6. Conclusions

As discussed above, the structures reported here for DB10 and DB12 represent the first accurate and reliable determination of the conventional low-

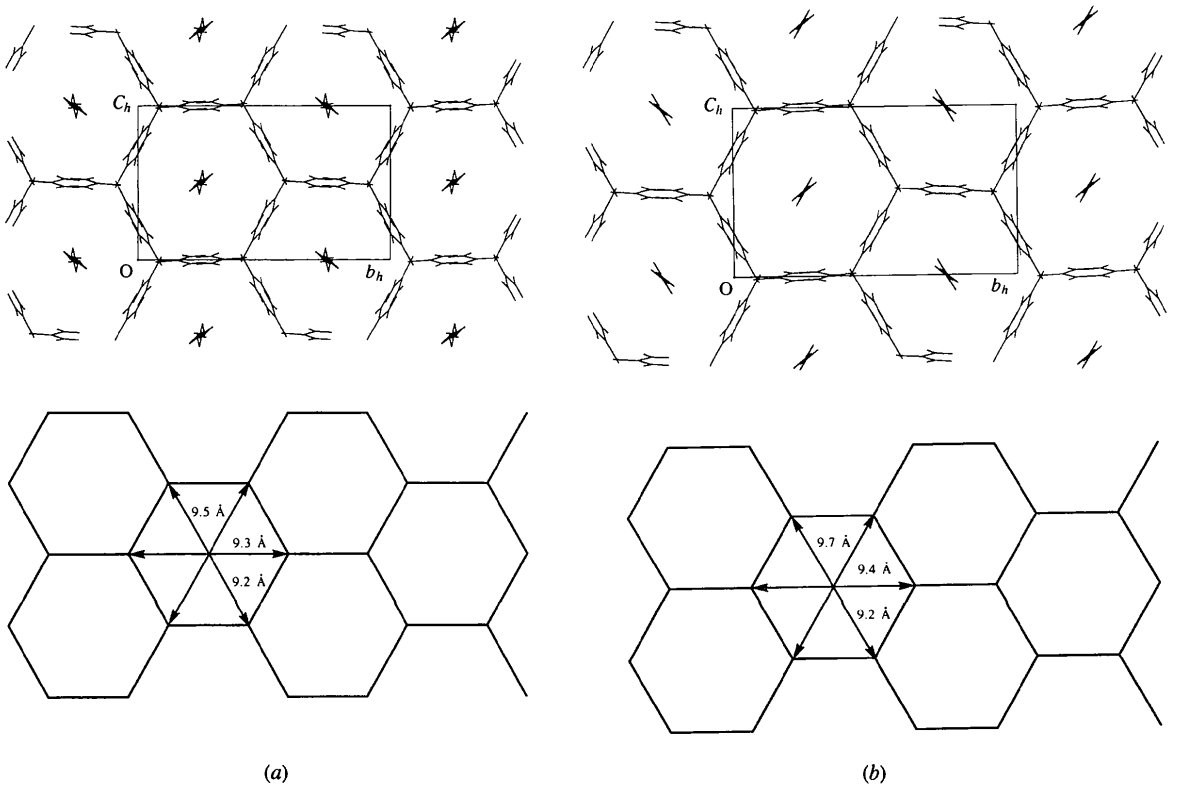

Fig. 3. Structures of the low-temperature phase at 108 K of (*a*) DB10 and (*b*) DB12, viewed along the tunnel axis (crystallographic *a* axis). The atoms within the tunnel (C4–C10) represent the contribution to the '*h*' diffraction pattern from scattering by the guest molecules (the physical significance of these atom positions is discussed in the text). The schematic diagrams show the geometrical characteristics of the host tunnel structure.

Table 2. *Fractional atomic coordinates and equivalent isotropic displacement parameters (Å²)*

$U_{eq} = (1/3)\Sigma_i\Sigma_j U^{ij} a_i^* a_j^* \mathbf{a}_i.\mathbf{a}_j.$

	x	y	z	U_{eq}
DB10 RT				
O1	0.6406 (7)	0.3203 (4)	0.0833	0.039 (2)
N1	0.9125 (7)	0.4344 (7)	0.1862 (4)	0.045 (2)
C1	0.8183 (11)	0.4092 (6)	0.0833	0.035 (2)
C2	0.9511 (36)	0.0000	0.0000	0.183 (10)
C3	1.0093 (57)	0.0047 (28)	0.0833	0.231 (14)
DB12 RT				
O1	0.6405 (7)	0.3203 (3)	0.0833	0.041 (2)
N1	0.9125 (7)	0.4347 (7)	0.1864 (4)	0.048 (2)
C1	0.8172 (10)	0.4086 (5)	0.0833	0.033 (2)
C2	−0.0152 (35)	0.0005 (72)	0.0389 (21)	0.239 (9)
DB10 LT				
O1	0.3318 (5)	0.0918 (4)	0.0345 (6)	0.0366 (13)
O2	0.9993 (4)	0.0685 (3)	0.0132 (6)	0.0303 (12)
O3	0.6650 (4)	0.0899 (3)	−0.0129 (5)	0.0276 (11)
N11	0.2295 (5)	0.0069 (5)	−0.1619 (8)	0.0284 (14)
N12	0.4383 (6)	0.0346 (6)	−0.1837 (8)	0.044 (2)
N21	1.1044 (5)	0.2080 (5)	0.0246 (9)	0.042 (2)
N22	0.8981 (6)	0.2054 (4)	−0.0218 (9)	0.034 (2)
N31	0.5649 (5)	0.0318 (4)	0.2087 (8)	0.0255 (14)
N32	0.7696 (6)	0.0134 (5)	0.1846 (8)	0.038 (2)
C1	0.3295 (7)	0.0443 (6)	−0.1030 (9)	0.034 (2)
C2	0.9993 (6)	0.1580 (5)	0.0037 (10)	0.033 (2)
C3	0.6613 (6)	0.0473 (5)	0.1212 (8)	0.0261 (15)
C4	0.5789 (23)	−0.2274 (13)	−0.0134 (24)	0.090 (4)
C5	0.4115 (16)	−0.2044 (11)	0.0566 (20)	0.089 (4)
C6	0.7434 (16)	−0.2562 (13)	−0.0758 (25)	0.098 (5)
C7	0.3990 (19)	−0.2575 (15)	−0.0108 (27)	0.112 (6)
C8	0.6157 (49)	−0.2645 (40)	−0.0071 (62)	0.271 (28)
C9	0.2588 (20)	−0.2568 (15)	−0.0191 (31)	0.119 (6)
C10	0.5220 (50)	−0.2455 (48)	−0.0106 (55)	0.282 (29)
DB12 LT				
O1	0.3348 (4)	0.0895 (3)	1.0370 (5)	0.0360 (10)
O2	1.0001 (3)	0.0683 (3)	1.0150 (5)	0.0356 (11)
O3	0.6673 (4)	0.0913 (3)	0.9911 (5)	0.0352 (10)
N11	0.2291 (5)	0.0075 (4)	0.8414 (6)	0.0377 (14)
N31	0.5629 (4)	0.0344 (4)	1.2098 (7)	0.0358 (13)
N12	0.4365 (4)	0.0307 (5)	0.8187 (7)	0.044 (2)
N21	1.1029 (4)	0.2074 (3)	1.0258 (7)	0.0367 (13)
N22	0.8951 (4)	0.2054 (4)	0.9812 (8)	0.050 (2)
N32	0.7702 (5)	0.0130 (4)	1.1898 (7)	0.0409 (15)
C1	0.3325 (5)	0.0448 (5)	0.9026 (7)	0.0356 (14)
C2	0.9987 (5)	0.1580 (5)	1.0060 (7)	0.0347 (15)
C3	0.6656 (6)	0.0473 (4)	1.1263 (7)	0.0307 (13)
C4	0.8355 (23)	0.7594 (13)	0.0182 (22)	0.130 (5)
C5	0.4735 (26)	0.7328 (17)	−0.0288 (29)	0.162 (8)
C6	0.6333 (30)	0.7553 (17)	0.0084 (30)	0.152 (8)
C7	0.5617 (31)	0.7472 (20)	−0.0068 (36)	0.164 (9)
C8	0.7622 (35)	0.7215 (28)	−0.0876 (56)	0.302 (20)
C9	0.7366 (28)	0.7599 (15)	0.0269 (33)	0.156 (8)
C10	0.9398 (37)	0.7101 (27)	−0.0509 (47)	0.276 (16)

Table 3. *Selected geometric parameters (Å, °)*

DB10 RT			
O1—C1	1.273 (10)	N1—C1	1.337 (6)
O1—C1—N1^{i}	120.3 (4)	N1^{i}—C1—N1	119.4 (7)
DB12 RT			
O1—C1	1.258 (9)	N1—C1	1.336 (5)
O1—C1—N1^{i}	120.5 (3)	N1^{i}—C1—N1	119.0 (7)
DB10 LT			
O1—C1	1.293 (8)	N21—C2	1.361 (9)
O2—C2	1.251 (9)	N22—C2	1.312 (9)
O3—C3	1.236 (8)	N31—C3	1.293 (9)
N11—C1	1.308 (9)	N32—C3	1.381 (10)
N12—C1	1.371 (10)		
O1—C1—N11	122.3 (7)	N22—C2—N21	118.9 (7)
O1—C1—N12	116.3 (7)	O3—C3—N31	125.9 (6)
N11—C1—N12	121.5 (7)	O3—C3—N32	117.4 (6)
O2—C2—N22	120.8 (7)	N31—C3—N32	116.7 (6)
O2—C2—N21	120.2 (7)		
DB12 LT			
O1—C1	1.268 (7)	N12—C1	1.342 (8)
O2—C2	1.271 (8)	N21—C2	1.346 (7)
O3—C3	1.270 (7)	N22—C2	1.331 (8)
N11—C1	1.344 (8)	N32—C3	1.347 (8)
N31—C3	1.326 (8)		
O1—C1—N11	122.3 (5)	N22—C2—N21	118.5 (6)
O1—C1—N12	120.1 (5)	O3—C3—N31	122.0 (6)
N11—C1—N12	117.6 (5)	O3—C3—N32	120.0 (5)
O2—C2—N22	121.4 (5)	N31—C3—N32	118.0 (5)
O2—C2—N21	120.0 (5)		

Table 4. *Atomic coordinates of the host structure in the 1,10-dibromodecane–urea inclusion compound at ambient temperature based on the orthohexagonal cell* $[a_h(o) = 8.271, b_h(o) = 14.326, c_h(o) = 11.083\,Å]$

Comparison with the atomic coordinates for the urea molecules given in Table 3 confirms that the change in the host structure upon entering the low-temperature phase represents a rather small structural distortion.

	$x/\lvert a_h(o)\rvert$	$y/\lvert b_h(o)\rvert$	$z/\lvert c_h(o)\rvert$
O1	0.33	0.09	0.02
O2	1.00	0.07	0.00
O3	0.67	0.09	−0.02
N11	0.23	0.01	−0.17
N12	0.44	0.03	−0.20
N21	1.10	0.21	0.02
N22	0.90	0.21	−0.02
N31	0.56	0.03	0.20
N32	0.77	0.01	0.17
C1	0.33	0.05	−0.11
C2	1.00	0.16	0.00
C3	0.67	0.05	0.11

temperature structure of urea inclusion compounds. Importantly, this structure is also exhibited by the prototypical alkane/urea inclusion compounds. As the vast majority of reported studies of the low-temperature phase transition in urea inclusion compounds have been for the alkane/urea and α,ω-dibromoalkane/urea inclusion compounds, the structural information on the low-temperature phase determined here provides a basis for rationalization of structural aspects of the phase transition. Indeed, now that reliable and accurate knowledge of the conventional low-temperature structure of these inclusion compounds is available, we forecast with confidence that future theoretical and computational studies will lead to significant progress in deriving a fundamental understanding of the low-temperature phase transition in urea inclusion compounds.

It is interesting to comment upon the fact that for the DB10 and DB12 inclusion compounds the transformation from the high-temperature phase to the low-temperature phase occurs in a single crystal to single crystal manner, whereas for alkane/urea inclusion compounds a single crystal in the high-temperature phase becomes multiply twinned on passing below the phase transition temperature. Thus, for a single crystal of DB10 or DB12 the same mode of distortion of the tunnel

structure occurs throughout the whole crystal, whereas for an alkane/urea crystal, orientationally different (but otherwise equivalent) distortions of the tunnel structure presumably occur in different parts of the parent crystal. These differences may originate from the fact that the mode of three-dimensional ordering of the guest molecules in α,ω-dibromoalkane/urea inclusion compounds ($\Delta_g = c_g/3$) is different from the mode of three-dimensional ordering of the guest molecules in alkane/urea inclusion compounds ($\Delta_g = 0$), or perhaps from the subtle difference noted recently (Aliev, Smart, Shannon & Harris, 1996) on the way in which the dynamics of the guest molecules change on crossing the phase transition temperature (the change is substantially more abrupt in the case of the alkane/urea inclusion compounds). However, in view of the limited evidence currently available, we do not speculate further on the retention of single crystal character on passing below the phase-transition temperature for DB10 and DB12 inclusion compounds in comparison with the multiple twinning that occurs for the alkane/urea inclusion compounds.

Finally, although the conventional low-temperature structure reported here is exhibited by urea inclusion compounds containing alkane and α,ω-dibromoalkane guest molecules, we have discovered recently (Yeo, Harris & Guillaume, 1997) that the 1,10-decanedicarboxylic acid/urea inclusion compound has a different structure in its low-temperature phase (note that this inclusion compound has the conventional hexagonal urea tunnel structure at ambient temperature). Again, the development of a comprehensive understanding of the anomalous structural behaviour of this inclusion compound at low temperature presents a challenging problem for future research.

We are grateful to Ciba Specialty Chemicals and the University of Birmingham for providing studentships (to LY) and to EPSRC for general support.

References

Aliev, A. E., Smart, S. P., Shannon, I. J. & Harris, K. D. M. (1996). *J. Chem. Soc. Faraday Trans.* **92**, 2179–2185.

Brown, M. E., Chaney, J. D., Santarsiero, B. D. & Hollingsworth, M. D. (1996). *Chem. Mater.* **8**, 1588–1591.

Brown, M. E. & Hollingsworth, M. D. (1995). *Nature*, **376**, 323–327.

Burla, M. C., Camalli, M., Cascarano, G., Giacovazzo, C., Polidori, G., Spagna, R. & Viterbo, D. (1989). *J. Appl. Cryst.* **22**, 389–393.

Casal, H. L., Cameron, D. G. & Kelusky, E. C. (1984). *J. Chem. Phys.* **80**, 1407–1410.

Chatani, Y., Anraku, H. & Taki, Y. (1978). *Mol. Cryst. Liq. Cryst.* **48**, 219–231.

Chatani, Y., Taki, Y. & Tadokoro H. (1977). *Acta Cryst.* B**33**, 309–311.

El Baghdadi, A., Dufourc, E. J. & Guillaume, F. (1996). *J. Phys. Chem.* **100**, 1746–1752.

Flack, H. D. (1983). *Acta Cryst.* A**39**, 876–881.

Fukao, K. (1990). *J. Chem. Phys.* **92**, 6867–6874.

Guillaume, F., Sourisseau, C. & Dianoux, A.-J. (1991). *J. Chim. Phys. (Paris)*, **88**, 1721–1739.

Harris, K. D. M. (1993). *J. Solid State Chem.* **106**, 83–98.

Harris, K. D. M., Gameson, I. & Thomas, J. M. (1990). *J. Chem. Soc. Faraday Trans.* **86**, 3135–3143.

Harris, K. D. M. & Jonsen, P. (1989). *Chem. Phys. Lett.* **154**, 593–598.

Harris, K. D. M., Smart, S. P. & Hollingsworth, M. D. (1991). *J. Chem. Soc. Faraday Trans.* **87**, 3423–3429.

Harris, K. D. M. & Thomas, J. M. (1990). *J. Chem. Soc. Faraday Trans.* **86**, 2985–2996.

Hollingsworth, M. D., Brown, M. E., Hillier, A. C., Santarsiero, B. D. & Chaney, J. D. (1996). *Science*, **273**, 1355–1359.

Hollingsworth, M. D. & Harris, K. D. M. (1996). *Comprehensive Supramolecular Chemistry*, edited by D. D. MacNicol, F. Toda & R. Bishop, Vol. 6, pp. 177–237. Oxford: Pergamon Press.

Hollingsworth, M. D., Harris, K. D. M., Chaney, J. D., Werner-Zwanziger, U., Huffman, J. C., Smart, S. P. & Santarsiero, B. D. (1997). Manuscript in preparation.

Hollingsworth, M. D., Santarsiero, B. D. & Harris, K. D. M. (1994). *Angew. Chem. Int. Ed. Engl.* **33**, 649–653.

Johnson, C. K. (1976). *ORTEP*II. Report ORNL-5138. Oak Ridge National Laboratory, Tennessee, USA.

Lefort, R., Etrillard, J., Toudic, B., Guillaume, F., Breczewski, T. & Bourges, P. (1996). *Phys. Rev. Lett.* **77**, 4027–4030.

Lynden-Bell, R. M. (1993). *Mol. Phys.* **79**, 313–321.

Molecular Structure Corporation (1993). *TEXSAN. Single Crystal Structure Analysis Software*. MSC, 3200 Research Forest Drive, The Woodlands, TX 77381, USA.

Parsonage, N. G. & Pemberton, R. C. (1967). *Trans. Faraday Soc.* **63**, 311–328.

Pemberton, R. C. & Parsonage, N. G. (1965). *Trans. Faraday Soc.* **61**, 2112–2121.

Pemberton, R. C. & Parsonage, N. G. (1966). *Trans. Faraday Soc.* **62**, 553–557.

Rigaku Corporation (1994). *R-Axis*II *Software*. Rigaku Corporation, Tokyo, Japan.

Smart, S. P., Guillaume, F., Harris, K. D. M. & Dianoux, A.-J. (1994). *J. Phys. Condens. Matter*, **6**, 2169–2184.

Sheldrick, G. M. (1993). *SHELX*93. *Program for Crystal Structure Determination*. University of Cambridge, England.

Smith, A. E. (1952). *Acta Cryst.* **5**, 224–235.

Smaalen, S. van (1995). *Crystallogr. Rev.* **4**, 79–202.

Smaalen, S. van & Harris, K. D. M. (1996). *Proc. R. Soc. London Ser. A.* **452**, 677–700.

Yeo, L., Harris, K. D. M. & Guillaume, F. (1997). *J. Solid State Chem.* **128**, 273–281.